DISSERTATION

On

Synthesis and Characterization of Lanthanum Doped Strontium Titanate by Sol Gel Route

Submitted in partial fulfillment of the requirement

for the award of degree of

Master of Technology

in

Material Science and Metallurgical Engineering

Submitted By :

DHARAM PAL SINGH

Roll No. 601102012

Under The Guidance of

Dr. DWIJENDRA P. SINGH

Assistant Professor

Department of SPMS

Thapar University, Patiala

SCHOOL OF PHYSICS AND MATERIAL SCIENCE

THAPAR UNIVERSITY

PATIALA-147004, INDIA

JULY-2013

This Thesis is dedicated to

My Parents

DECLARATION

I hereby declare that work done in this Thesis Report entitled, **"Synthesis and Characterization of Lanthanum Doped Strontium Titanate by Sol Gel Route"** submitted towards partial fulfillment of requirement for award of **Master of Technology** degree in **Material Science & Metallurgical Engineering** in **School of Physics & Material Science** of **Thapar University, Patiala,** is an authentic record of work carried out by me under the supervision and guidance of **Dr. Dwijendra P. Singh, Assistant Professor** of **School of Physics & Material Science, Thapar University, Patiala.**

This matter embodied in this report has not been submitted in part or full to any other university or institute for the award of any degree.

Dharam Pal Singh

This is to certify that above declaration made by the student concerned is correct to the best of my knowledge & belief.

Dr. Dwijendra P. Singh
Assistant Professor
Mechanical Engineering Department
Thapar University, Patiala

Countersigned by:

Dr. Kulvir Singh
Professor & Head of the Department
School of Physics & Material Science
Thapar University, Patiala

Dr. S.K. Mohapatra
Sr. Prof & Dean of Academic Affairs
Mechanical Engineering Department
Thapar University, Patiala

iii | P a g e

ACKNOWLEDGEMENT

I take the opportunity to express my heartfelt adulation and gratitude to my supervisor Dr. Dwijendra P. Singh for his unreserved guidance, constructive suggestions, thought provoking discussions and unabashed inspiration in the nurturing work. It has been a benediction for me to spend many opportune moments under the guidance of the perfectionist at the acme of professionalism. The present work is testimony to his activity, inspiration and ardent personal interest, taken by him during the course of his work in its present form. I am grateful to Dr. Kulvir Singh, Professor and Head, School of Physics & Material Science for providing the facilities for the completion of the work and always being a shelter in the odd days.

I am also very much indebted for valuable suggestion provided by Dr. Bhasker Gahtori, Mr. B. Sivaiah (Scientists at NPL Delhi).

I am also thankful to the Ph. D. scholars Pallvi Gupta, Mintu Tyagi, Kriti Tyagi and Suresh Kumar. The greatest thanks go to my Parents for their infinite support. Above all, I express my indebtedness to the "ALMIGHTY" for all His blessing and kindness.

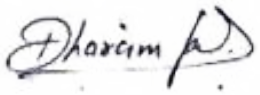

Dharam Pal Singh
601102012
SPMS

ABSTRACT

The La doped $SrTiO_3$ with varying stoichiometric compositions ($La_{0.1}Sr_{0.9}TiO_3$, $La_{0.02}Sr_{0.98}TiO_3$, $La_{0.04}Sr_{0.96}TiO_3$, $La_{0.06}Sr_{0.94}TiO_3$) has been successfully amalgamated using the Sol-Gel method which has not been used much for this particular ceramic. The LSTO samples under study have been subjected to structural, morphological and localized chemical analysis using XRD, SEM and EDS analysis respectively. The XRD studies pointed towards the single phase presence for all samples, same value of lattice parameter shows cubic structure and crystalline size and lattice parameter decreases w.r.t increment in lanthanum doping. The SEM studied showed the good morphological structure with average grain size of the particles around 2–3 μm. The SEM analysis of pallets made by Spark Plasma Sintering showed that with sintering 1200^oC have less porosity and good compactness as compared to the pallet sintered at 1000^oC. The EDS study was performed on one point at local areas of every sample, the measured La concentration which was almost the same the stoichiometric ratio for all value of x (x = 0.1, 0.02, 0.04, 0.06) in $La_xSr_{1-x}TiO_3$.

LIST OF ABBREVIATIONS

CPD	Committee on Powder Diffraction
DTA	Differential Thermal Analysis
EDAX	Energy Dispersive X-Ray Spectroscope
EDS	Electron Dispersive Spectroscopy
ICDD	International Center for Diffraction
LSTO	$LaSrTiO_3$
P-E	Polarised Electric Field
PXRD	Powder X-ray Diffraction
RP	Ruddlesden Popper Structure
SEM	Scanning Electron Microscopy
SLTO	$Sr_{0.92}La_{0.08}TiO_3$
SPS	Spark Plasma Sintering
SRTO	$Sr_{0.95}$ R $_{0.05}TiO_3$
SSR	Solid State Reaction
STO	$SrTiO_3$
TE	Thermoelectric
XRD	X-Ray Diffraction
ZT	Figure of Merit

NOMENCLTURE

A,B	Cation
d	Interspacing Distance
K	Shape Factor
κ_{total}	Total Thermal Conductivity
λ	Wavelength
m*	Carrier Effective Mass
m_0	Mass of Electron
n	Integer
ρ	Density
r	Ionic Radius
S	Seeback Coefficient
t	Tolerance Factor
τ	Relaxation Time
T_C	Curie Temperatures
T_{cal}	Calcining Temperature
θ	Bragg Angle
X	Anion (Oxygen)

LIST OF FIGURES

LIST OF TABLES

TABLE OF CONTENTS

CHAPTER1

INTRODUCTION

In this chapter the structure of perovskite (ABO_3), STO ($SrTiO_3$) perovskite material and the different doping elements which can be added into STO are being discussed along with their different properties and applications.

1.1 GENERAL

In the ongoing era material science have a great importance in our society, and for advanced technological developments that is dependent upon the latest upgraded materials with desired properties [1]. To develop new material for the suitable quality, it is very necessary to understand the coloration between the atomic scale structure, synthesis and bulk properties.

Perovskites types of structure materials attract because of extensive research due to their great properties. These ceramic materials having general formula ABX_3, where A is mostly a group I-II element and B is mostly a transition metal. B and A are cation (A-site is occupied by large and B-site occupied smaller cation) and X is anion, X in most cases will be oxygen. By replacement with different doping of cations in A-site and B-site in perovskite structure bring a range of properties, so from this point of view we can say that the perovskite structure have tailor-made qualities [2]. The tailor-made ability of perovskite structure ceramic materials is responsible for development of new oxide materials.

The background of perovskite structure start with Calcium titanate ($CaTiO_3$), this is a natural mineral material was described in 1839 by Gustav Rose. Gustav Rose titled this structure in the honor of a Russian mineralogist Count Lev Alexejevitj Perovskii. The common example of perovskite is $SrTiO_3$ (STO) as described as ideal perovskite structure [2].

1.2 PEROVSKITE STRUCTURE

The general formula of perovskite (ABX_3), A and B are cations, B is smaller than A and X and X-site position of anion similar in size of A-cation. Octahedrons (BX_6) forms at the corners of the structure and A in the center of the cube in

interstitial-site surrounded by twelve X-anions in cub octahedral coordination, and B in the center of the octahedrons-site surrounded by six X-anions at the corners [3] as shows in Fig. 1.1.

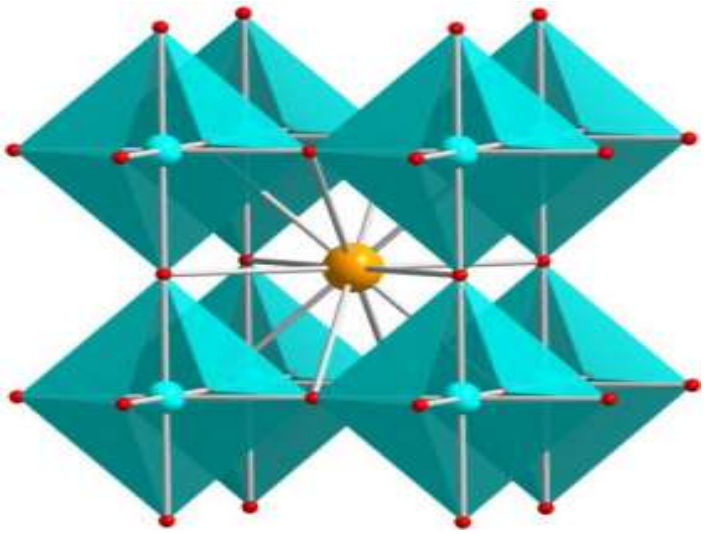

Fig. 1.1 The ideal perovskite structure (B-cell setting) A-site (yellow), B and X-site shows blue and red.

There is different ways to represent the perovskite structure. A-site at the origin and B-site at the origin, in Fig. 1.1 and 1.2 (a) shows the B-cell setting and A-cell setting type of representation. In A-cell setting A at the origins of the unit cell and B-site placed at center of the unit cell, and X-site on the face center of the each face. In other hand in B-cell setting B-site at the origin of the unit cell and the X-site at the middle of the edges, and A at center of unit cell.

1.2.1 Tolerance Factor

In 1926 Goldschmidt[4] found that at the certain conditions of temperature and pressure , the assembly of ions will form an ideal perovskite structure could be explained by a relative ratio of the ionic radii of ABO_3 known as tolerance factor (t):

$$t = \frac{(r_A + r_X)}{\sqrt{2}(r_B + r_X)} \qquad (1.1)$$

where r_A, r_B, r_X is the ionic radius of atom A, B and X. if ABX_3 has t =1, r_A= 1.44Å and r_B= 605.0Å, r_X = 40.1Å cubic perovskite is ideal structure, on the other

side the t <1 and if the A ion is less than the ideal value of ionic radii or if the B ion have the large value, the result is BO_6 octahedral atoms will tilt in order to occupy the space and the symmetry of the crystal structure is lowered and in the another case if t >1 due to a large A or small B ion then tetragonal and hexagonal variation of the perovskite structure will be stable. The perovskites are not truly ionic compounds and since the values are taken for the ionic radii [4] the tolerance factor is just a rough estimation for giving an idea for compounds with a high degree of ionic bonding.

1.3 STRONTIUM BASED OXIDE

STO based oxides are perovskite-type: (a) STO, (b) a layered perovskite type Ruddlesden Popper (RP) phase of STO and (c) a $SrTiO_3/SrTiO_3$: Nb super-lattice. STO-based oxide are a promising group of n-type TE (thermoelectric) materials cause of these materials exhibits outstanding transport properties and the big thing is stable at high temperature but thermally conductive in nature [5].

1.3.1 Physical Properties of STO

Non doped $SrTiO_3$ (STO) is an insulator and its resistivity at room temperature is above of 10^{13} Ω cm and wide band gap 3.2 eV within 2p band of oxygen and the 3d band of titanium [6] physical properties of this material are printed into given in Table 1.1.

$SrTiO_3$ (STO) with band gap of ~3.2 eV, is a typical band insulator. Wide Insulating STO dielectrics shows a singular dielectric behavior and the quantum paraelectric behavior, i.e. its dielectric permittivity continuously increases with decreasing temperature up to 4 K, and after that remains constant below the 0.03 K. However, there is some dielectric peaks were observed in STO doped with a small amount of calcium or bismuth [7] which were clarified that the impurity induced ferro-electricity or polar cluster effect inside the doped STO material.

On the other side, the electrical transport activities in STO has appealed much attention, due to the occurrence of the superconductivity in Nb-doped or oxygen deficient STO, which was first experientially proved more than 30 years ago [8] and the La doping also causes the superconductivity in STO.

Table 1.1 physical properties of $SrTiO_3$

Properties	**Values**
Lattice parameter at RT (nm)	0.3905
Atomic density (g/cm^3)	5.12
Melting point (°C)	2080
Mohs hardness	6
Dielectric constant (ε_0)	300
Thermal conductivity (W/m.K)	12
Coefficient of thermal expansion (ppm/°C)	9.4×10^{-6}
Refractive index	2.31-2.38

1.3.2 Crystal Structure and Bonding

$SrTiO_3$ crystallizes at room temperature, in the ABO_3 cubic perovskite structure having density of $\rho = 12.5$ g/cm^3 and lattice parameter of 0.3905 nm. In a unit cell one Ti^{4+} ions surrounded by six O^{2-} ions, and every Sr^{2+} ions is enclosed by four TiO_6 octahedral atoms, so each Sr^{2+} ion is coordinated by 12 O^{2-} ions. Within the TiO_6 octahedral atoms, and there is hybridization of the Ti-3d states with the O-2p states have covalent bonding in other side O^{2-} and Sr^{2+} ions exhibit ionic bonding [9]. Hence, $SrTiO_3$ has mixed bonding properties (ionic-covalent). This type of bonding shows the unique type of structure.

STO has an isotropic cubic crystal structure (Fig.1.2 (a)), which has a so strong structural tolerance towards doping as to reach a degenerate state possessing a high electrical conductivity, and is known to have an electronic band structure in which the conduction band is made of the Ti 3d orbitals consisting of triply degenerate orbitals (3dxy, 3dyz and 3dxz) in the cubic TiO_6 octahedral atoms (Fig.1.2 (b)).

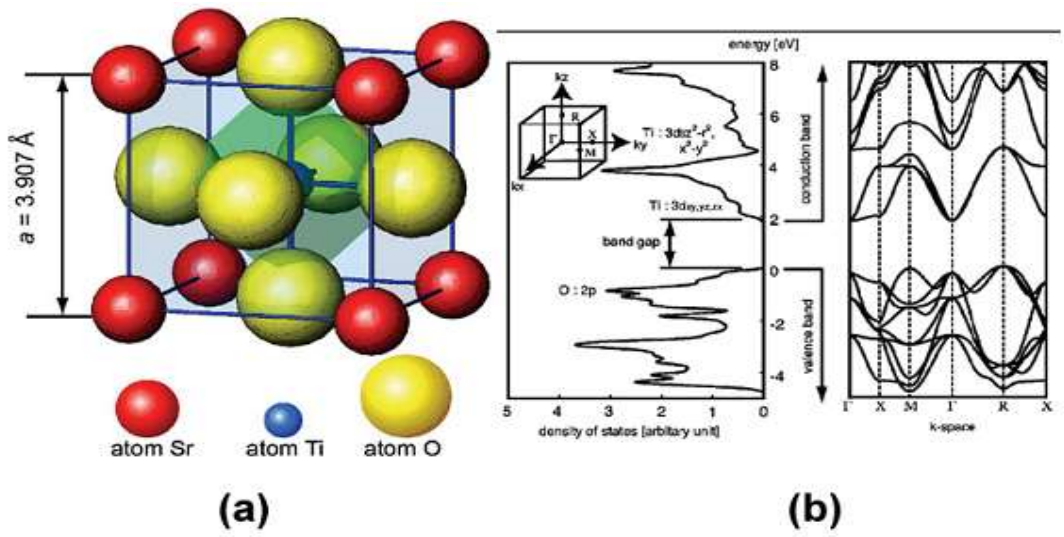

Fig. 1.2 (a) Crystal structure of $SrTiO_3$, (b) The band structure and the density of states of the cubic phase of $SrTiO_3$ [10]

The basic perovskite structure of material is ideal to analyzing the electronic structure of linear metal-oxygen-metal bonds of octahedral coordinated metal ions. Direct interaction of metal-metal is can't be possible because of an oxygen atom present in the path of two titanium neighbor's atoms. Oxygen-oxygen interactions are relatively weak, since oxygen-oxygen bonding distances twice of the titanium-oxygen bond lengths. In $SrTiO_3$, the effect of the strongly ionized and electronically strontium ion on the titanium-oxygen covalent bond is minor. The electronegativity of Strontium is very low (1.0) [11] has transferred electrons to the TiO_3, and does not fight for electrons.

To analyze the carrier-doping effects on the tolerance factor (t) and the ionic radii, the examination of bottom of the conduction band and of the top of the valence band of the component is necessary. As shown in Fig.1.2, the top of the valence band consists of O-2p orbitals, while the bottom of the conduction band of $SrTiO_3$ is composed of Ti-3d orbitals. The electron cloud will be increase around the Ti atom because of the doped electrons accommodated in the Ti-3d orbitals, and increasing the radii of the Ti ion. Because of expansion in the radius of the Ti ion leads to the smaller tolerance factor, and therefore to the promotion of the TiO_6-octahedron rotating instability.

$$t = \frac{(r_{Sr} - r_O)}{\sqrt{2}(r_{Ti} - r_O)} = \frac{1}{\sqrt{2}}\left(1 + \frac{(r_{Sr} - r_{Ti})}{(r_{Ti} - r_O)}\right) \quad (1.2)$$

in the next side, because of the doped holes captured at the O-2p orbitals lead to the decreased electron clouds around the O atoms, and therefore the contraction in the radius of the O ion, and (r_{Sr}- r_{Ti}) have positive value, the smaller radii of O produced the higher tolerance factor [10] and therefore in the suppression of the TiO_6-octahedron rotating instability.

1.3.3 Electron doping

The main purpose of doping is the establishment or introduces an electrically active n or p type dopants to enhancement of the free carrier concentration [12].

In the case of $SrTiO_3$ the most significant criterion for a possible replacement of Strontium or Titanium site ions by doped element is a similar ionic radius of the equivalent species. Dopants with a lower or higher oxidation level than the host ion act as acceptors or donor. When these dopants are lighter or of neighboring masses to the host elements or at lower concentration, then ion beam techniques are notable to determine the implant site, when the "emission channeling radioactive nuclear technique" shall be used [13]. In the following some examples for each type of dopant are given.

- Possible donors: Trivalent ions such as $Al^{3+,}$ La^{3+}ions on Sr^{2+} sites or pentavalent ions such as Nb^{5+}, Ta^{5+} ions on Ti^{4+}sites act as single donors.
- Possible acceptors: Fe^{3+} as trivalent ions on Ti^{4+} sites, or Na^{1+} as monovalent dopant on Sr^{2+} sites, may act as single acceptors.
- Amphoteric: Group Ib elements can act as donors or acceptors.

Doping material could be used to modify the electrical properties of the material. Dopants behave in different ways which is depending on their ionic radii and valiancy shell, as dopants like Niobium, Lanthanum and iron have been preferred in this work.

Table 1.2 Crystal and ionic radii of Sr, Ti and the most common dopants for $SrTiO^3$ [12].

Ion	Coordination	Crystal radius [Å]	Ionic radii [Å]
Sr^{2+}	XII	1.58	1.44
Ti^{4+}	VI	0.75	0.61
La^{3+}	XII	1.50	1.36
Fe^{3+}	VI	0.69	0.55
		0.79	0.65
Nb^{5+}	VI	0.78	0.64

$La^{3+}$and Nb^{5+} behave as donors, whereas Fe^{3+} substitutes for Ti^{4+} acts as acceptor, since La^{3+} occupies the Sr^{2+} site and Nb^{5+} the Ti^{4+} site.[14]The behavior of the cations as per their ionic radii which are printed in the Table 1.2.

1.4 APPLICATIONS OF STO.

Strontium Titanate (STO) is an excellent material for electro-ceramic oxides materials, because of its chemical and thermal stability and its well understandable defect chemistry. Its defect structure is same as the other perovskites materials those are highly relevance as positive temperature coefficient resistors, capacitors and dielectrics in microelectronics devices.[13] STO also applicable for high-temperature superconductors and anode in solid oxide fuel cells [14] within 750°C and 950°Ctemperature range with the oxygen partial pressure ranging between 1 and 10^{-5}bar, the resistance of the solid solution $SrTi_{0.65}$ $Fe_{0.35}O_{3-\delta}$ is independent from the temperature and it varies only with the oxygen partial pressure [17]. Therefore, this material is a good candidate for the development of temperature insensitive sensors.

The modification in STO material by doping for the p-type and n-type STO semiconductor can enhance the thermoelectric properties for thermoelectric power generation and solid state refrigeration (Fig. 1.3).

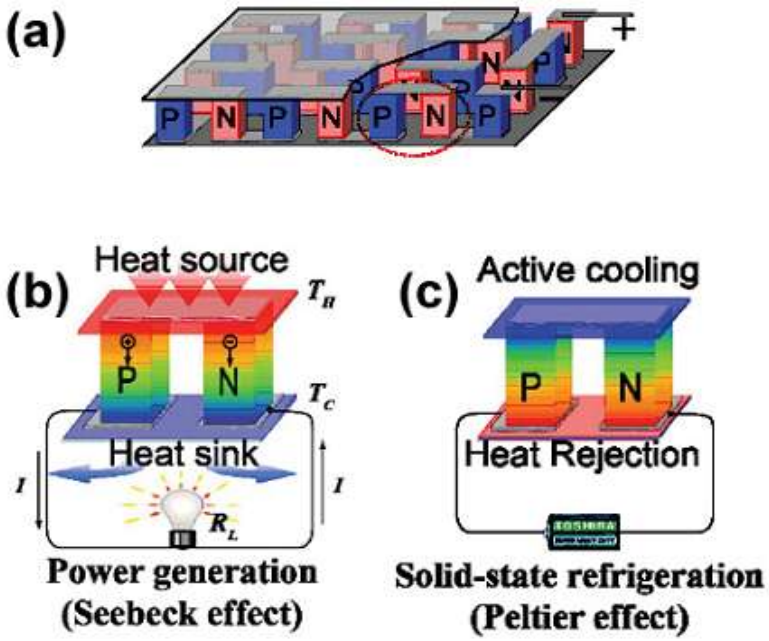

Fig.1.3 Schematic images of (a) a thermoelectric module assembled with quantities of n- and p-type thermoelectric elements, which can be used for (b) power generation and (c) solid-state refrigeration.

Doped STO materials are thermally conductive, the figure of merit for the polycrystalline and single-crystal are not greater than 0.37 at 1000 K, and the highest ZT expected for a conducting thin layer in the SrTiO3/SrTiO3:Nb super-lattice can be as large as 2.4 at room temperature [5]. However, for the practical applications, the TE performance of the bulk materials is still insufficient, and it remains a challenge to further improve their zT values.

1.5 POWDER SYNTHESIS METHODS

There is multiple range of routs have been used to synthesis the oxide ceramic powder. These are used for both industrial and laboratorial production. We can compare these methods on the basis of their processing routs and properties as shown in Table 1.3 [18-24].

1.5.1 Solid State Reaction

This is the widely used direct method of producing mixed oxide to react a mixture of metal oxide, hydroxide in the solid state. The ceramic powder is

Table 1.3 Comparison of oxide powder synthesis techniques

Synthesis Methods	Compo-sition Control	Morpho-logical Control	Particle Size (nm)	Purity (%)	Agglo-meration	Cost
Solid State Reaction	Moderate	Poor	>1000	<99.5	Moderate	Low moderate
Sol-Gel	Excellent	Moderate	> 10	> 99.9	Moderate	High Moderate
Spray Pyrolysis	Excellent	Excellent	>10	>99.9	Low	High
Hydro-thermal Synthesis	Excellent	Excellent	>10	>99.5	Low	Moderate
Coprecipi t-ation	Good	moderate	>10	>99.5	High	Moderate

prepared by solid state reaction in three steps is mixing, solid state reaction and milling. In the solid state reaction process results the formation of hard agglomerations that required a process to reduce the particle size to micro level is called comminution process, but technically it is very difficult to milling the material to produce the particle size below the 1µm [20]. In the solid state reaction the purity and homogeneity of the powder is very poor as compare to sol-gel and another methods, but particle size distribution is broad. The requirement of calcine the starting mixture at a higher temperature increases the costs of the synthesis.

1.5.2 Chemical Synthesis

The synthesis of oxide ceramic powders in chemical synthesis can support the purity, chemical homogeneity and lower processing temperatures due to of mixing of the starting materials in the solution state solution and the fine particle size can be produced. The chemical synthesis techniques are sol-gel method, spray pyrolysis and hydrothermal synthesis and last one Co-precipitation method.

1.5.2.1 Sol-Gel Method

The sol-gel rout consists of the preparation of an amorphous gel from solutions followed by dehydration at low processing temperatures. Since it starts from a solution of all components in the form of soluble compounds, the mixing at a molecular level is retained through gel formation [21]. The sol-gel method explained briefly in chapter 3.

1.5.2.2 Spray Pyrolysis

Spray drying differs and spray pyrolysis is deferent to each other in the use of solutions, the resultant process of condensation or precipitation within a droplet, and the use of significantly higher temperatures (>300ºC). During the spray pyrolysis, the solution is atomized into a series of reactors and the aerosol solvent evaporate and solute condensation within the droplet. At higher temperature the formation of the precipitate particle in the form of micro-porous material, and after the sintering process particle forms in the dense particle [22].

This process participates into the precipitation, calcination and sintering stages into single continues process which offered the great control on morphology.

1.5.2.3 Co-precipitation method

Co-precipitation from solution is an oldest wet chemical technique to produce the mixed oxides materials. In this method the preparation of an aqueous solution which comprises the precipitating agent, these precipitate products are replaced by filtration from the solution and after drying decomposed into preferred compound. For better results one has to control some parameters like pH value, concentration, processing temperature and the mixing rate. The desire properties like composition, purity and morphology have excellent results. Different rate of precipitation may cause of in homogeneity in the system [23]. This method can produce stoichiometric electro-ceramic powders with fine particle size and high purity at a comparatively moderate cost and is currently practically broadly to make electro-ceramic powders in industry

1.5.2.4 Hydrothermal synthesis

Hydrothermal synthesis can be well-defined as the action of aqueous solutions at higher temperature in high pressure vessels. It is an aqueous chemical process for synthesis of ceramic powders, when the reactant particles (oxides and hydroxides) of component oxides dissolve into aqueous solution, the precipitate out the product particles. The driving force in these reactions is the variance in solubility between the intermediate and oxide phase. The two major advantages of hydrothermal process are the elimination of the high temperature calcination process and the use of low expensive raw materials. Hydrothermal synthesis process for making ceramic powders can be easily distinguished from other process, such as the co-precipitation and sol- gel process by processing temperature and pressure used in this process [24]. The flow chart of hydrothermal process is given in Fig 1.4.

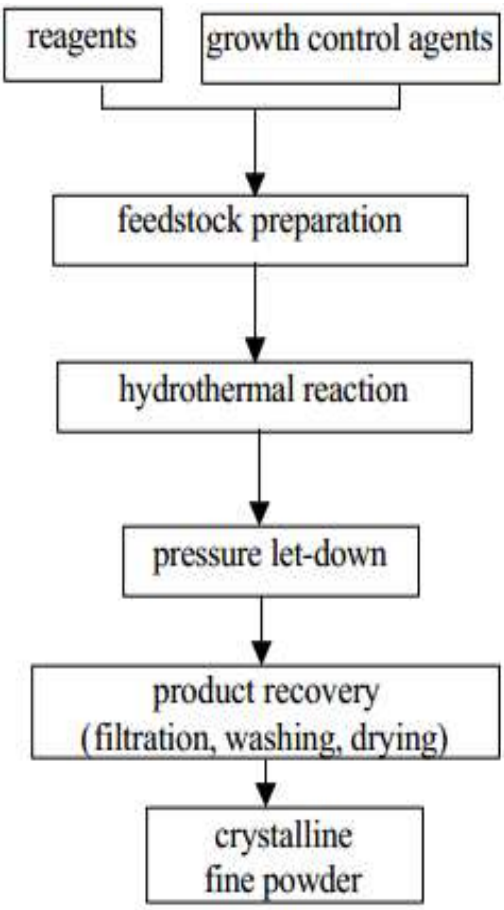

Fig. 1.4 Flow chart of hydrothermal synthesis process.

CHAPTER 2

LITERATURE REVIEW

In this chapter publications on the doped STO material, methods used in the literature, thermoelectric properties, sintering temperature and direction effect on thermoelectric properties, electronic structure and band gap are explained

Lui *et. al.*(2012) [25] tried to investigate the band behavior and thermoelectric properties of Dy doped $SrTiO_3$ceramics ($Sr_{x-1}Dy_xTiO_3$, x = 0.02, 0.05, 0.10) prepared by the reduced SSR (solid state reaction) method at room temperature to 973 K. All samples were found to consist of single phase with cubic structure, and for every sample resistivity enhanced with temperature which points towards there metallic behavior. The Seebeck coefficients saturated at high temperatures, with narrow band behavior validating ab initio calculations of the electronic structure, but the magnitudes of the Seebeck coefficient decreased with Dy content and similar trend was observed for electrical resistivity. The thermal conductivity showed decline with Dy content possibly due to reduction in lattice thermal conductivity by Dy substitution. The major conclusion which can be drawn is that a Seebeck coefficient was saturated at high temperatures values.

Qin *et. al.*(2012) [26] noticed the effect of calcining temperature (T_{cal}) and atmosphere on the phase composition of rare earth metal doped SrO $(SrTiO_3)_n$ oxides and noted the thermoelectric properties of bulk sample within temperature range of 300K-1000K. Solid-state reaction method with provision of Spark Plasma Sintering (SPS) technique was used for preparation of $(Sr_{0.95}R_{0.05})_3TiO_7$ (R= Eu, Nd) oxide. At T_{cal} temperature of 1500 ^oC the pure R-P phases powders were obtained with volume ratio of H_2 and Ar of about 5.95. The electrical resistivity (ρ) and the mode of negative Seebeck coefficient (S) values (|S|) showed rise with temperature pointing towards typical n-type degenerate semiconducting behavior, but the total thermal conductivity (κ_{total}) for all samples decreased with temperature which might be attributed to the enhancement in phonon at the internal interfaces of $SrO/SrTiO_3$. The major conclusion drawn was that Seebeck coefficient showed rise with temperature (for negative value mode was taken).

Wang *et. al.*(2011) [27] analyzed the thermoelectric properties of $SrTiO_3$while it was doped with lanthanum and dysprosium having concentration of $La_{0.1-x}Dy_{0.1+x}Sr_{0.8}TiO_3$ (x = 0.05, 0.02, 0.08, 0.10). Samples were prepared by conventional solid state reaction techniques. The materials consisted of dual phase, with one phase of $Dy_2Ti_2O_7$. SEM analysis of the samples showed absence of pores with both phases distributed homogeneously. The electrical conductivity and thermal conductivity decreased with dysprosium (Dy) content which was due to decrease in electronic thermal conductivity. The power factor declined due to fall in electrical conductivity as the Dy content increases. The maximum figure of merit (ZT) was found to be maximum (i.e. 0.36) in the sample with x = 0.02, which was even higher than that of the single lanthanum- or dysprosium-doped materials. Therefore, lanthanum and dysprosium dual-doping can effectively improve the thermoelectric properties of $SrTiO_3$ ceramics. The conclusion drawn from above discussion is that the lanthanum and dysprosium addition effectively improved thermoelectric properties of $SrTiO_3$ ceramics.

Wang *et. al.* (2010) [28] fabricated Pr-doped STO films and investigated their electrical properties, which were different from those of either pure STO films or Pr-doped ceramics. The difference in their properties can be well explained by the Pr-doping-induced changes in the microstructures and charge carriers. $Sr_{1-x}Pr_xTiO_3$ films were prepared by metal organic deposition method on (111) Pt/Ti/SiO2/Si substrates. Pr-doping greatly improves the dc leakage behavior of the films. The samples with x = 0.075 show excellent electric field frequency and temperature stability of dielectric properties, while the x = 0.025 samples indicate an obvious dielectric relaxation behavior and better polarization versus applied electric field (P-E) hysteresis loops. These weird electrical properties behavior of both samples can be explained mainly by the Pr-doping induced changes in the free charge carriers, the lattice distortion, the charge transfer process and polar nano-regions and the secondary reason might be that variable valence of Pr ions may also have significant impacts. The important conclusions drawn from above discussion were that Pr-doping assisted in enhancing the dc leakage behavior of films.

Okinaka *et. al.*(2010) [29] prepared rare earth doped with SRTO $Sr_{0.95}R_{0.05}TiO_3$ (R = La, Sm, Gd, Dy and Y) using amalgamation of combustion Synthesis and

Spark Plasma Sintering (SPS) and subsequently observed their thermoelectric properties. SEM results revealed that samples had homogeneous microstructures with few voids and small grains. The grain size varied in the range 2–10 mm. Another important observation made out was that with temperature the absolute value of Seebeck coefficient of all the samples increased but the electric conductivity decreased. In a considerable range of temperature the power factor of all the samples declined except Y-doped samples. Among all the samples, the La-doped sample and the Y-doped sample had the highest and lowest power factor respectively. The maximum figure of merit 0.22 was obtained at 800 K from $Sr_{0.92}La_{0.08}TiO_3$ sample. The thermoelectric properties of samples prepared using synthesis method in present study were relatively higher than samples prepared by conventional solid-state reaction methods. The conclusion drawn from present study was that the combination of combustion synthesis and spark plasma sintering had a full potential to prepare perovskite oxide materials having relatively higher thermoelectric properties and they can even be used for high-temperature applications.

Kinaci *et. al.* (2010) [31] in present study evaluated the power factor ($S^2\sigma$) for La-doped STO thin films and studied electronic transport properties of $SrTiO_3$ and for Bi_2Te_3 at 300 K and reports that $S^2\sigma$ for $SrTiO_3$ was at least 10 times than for Bi_2Te_3 at 300K. The reason cited for such discrepancy was not only due to La doping but also due to the oxygen deficiency of the STO substrates due deposition techniques of the thin films. The electronic transport properties of pure strontium titanate are also investigated. For the treatment of the substitutional alloys, on-site Coulomb interaction added versions of electronic exchange and correlation functional are preferred to obtain an accurate electronic band structure. Calculated Seebeck coefficient and its variation as a function of temperature for the alloy systems are compared with available experimental results; an excellent agreement is observed. Additionally, the electronic relaxation time and electronic contribution to thermal conductivity are predicted by fitting the calculated electrical conductivity to the experimental electrical conductivity. A significant increase in electronic thermal conductivity is observed for high carrier concentrations. Overall, the necessity of excessive carrier concentrations that can only be achieved by highly doped structures is verified.

Kikuchi *et. al*.(2009) [32] study the special effects of sintering temperature on the thermoelectric properties and microstructures of polycrystalline $Sr_{0.92}La_{0.08}TiO_3$ and also the effects of pressing direction during sintering on its thermoelectric properties and microstructures. The sample was prepared as same in previous publication and sintering with spark plasma sintering with longitudinal and transverse directions. They conclude that the average grain size of combustion-synthesized and spark-plasma-sintered SLTO increased with the sintering temperature. The maximum average grain size was 23.5 mm when sintering at 1663 K. Electric conductivity and microstructure of combustion synthesized $Sr_{0.92}La_{0.08}TiO_3$ were severely affected by the pressing direction during sintering. The combustion-synthesized powders were sintered well along the pressing direction during sintering, therefore the power factor measured along pressing direction during sintering was more than twice that measured perpendicular to the pressing direction during sintering in the experimental temperature range. The power factor of combustion-synthesized and spark plasma sintered SLTO was highest at the optimum sintering temperature of 1633 K because high-temperature sintering resulted in the introduction of oxygen defects and this oxygen defects produced electrons as carriers.

Liu *et. al.(*2009) [33] reported that enhancement of the Seebeck coefficient and ZT in oxygen-deficient $Sr_{1-x}\ La_x\ Ti_{3-\delta}$ bulk ceramics due to an introduced narrow conducting band. The S values of all oxygen-deficient samples are larger than those of the near-stoichiometric ones and are temperature-independent at high temperatures, showing a narrow band behavior. This indicates that the introduction of oxygen vacancy changes the density of electronic states around the Fermi energy. The maximum for the figure of merit (ZT) of $Sr_{1-x}\ La_x\ Ti_{3-\delta}$ceramic reaches 0.21 at about 750 K, demonstrating enhancement by a factor of more than 1.3 over that of the near-stoichiometric materials.

Yamada *et. al.*(2007) [34] studied the Parallel syntheses and thermoelectric properties of Ce-doped $SrTiO_3$ thin films. The thin film was grown in a pulsed laser deposition technique. They observe that using combinatorial pulsed-laser deposition TE properties of $Ce_xSr_{1-x}TiO_3$ films has been efficiently carried out. Temperature gradient method enabled to optimize growth temperature in single

experimental run. Composition-spread technique allowed high throughput characterizations of crystalline structure and thermoelectric properties, leading to rapid establishment of their composition dependences. They found that the present system has comparable TE properties to other electron-doped STO systems.

Voigts *et. al.(*2006) [35] study the sol-gel route for the production of un-doped and donor doped STO nanostructured thin films for sensor applications. They characterized these films by microscopic and electron spectroscopic methods. The films are produced by spin coating of a sol on silicon targets and subsequent annealing under ambient conditions. Analysis by atomic force microscopy shows particles with typical sizes between 10 nm and 50 nm. X-ray photoelectron spectroscopy displays a stoichiometry of the films as anticipated from preliminary experiments with strontium titanate single crystals. Metastable-induced electron spectroscopy and ultraviolet photoelectron spectroscopy are used as tools to give evidence to the similar electronic properties of nanoparticle film and single crystal. These results support the prospect for an application of the nanoparticle films as high temperature oxygen sensor with superior properties.

Ohta *et. al.(*2005) [36] focused on the effect of heavy doping of either Nb at the Ti site or La at the Sr site upon the carrier effective mass (m*). The Bulk single crystal samples of La doped STO or Nb doped STO had grown by a conventional Verneuil method at 2080ºC. The temperature dependence of μ and S changed at 750 K in all samples, indicating that the dominant carrier scattering mechanism changes with increasing temperature from a coupled scattering by polar optical phonons and acoustic phonons to mere acoustic phonon scattering. The thermal conductivity (k) of the samples, which was similar to that of un-doped SrTiO3 single crystal at room temperature, decreased proportionally to T^{-1},indicating that the lattice thermal conduction occurs predominantly. The m* of the Nb-doped STO (m* = 7.3-7.7m_0) is larger than that of La-doped STO (m* = 6.0-6.6m_0).

The reduced electric-charges by the doped carriers lead to the diminished electric-dipole moments and therefore the decreased energy gain by the long-

range Coulomb interactions among them, resulting in the suppression of the ferroelectric instability.

Uchida *et. al.*(2003) [8] studied carrier-doping effects in $SrTiO_3$ by the first-principles calculations. The modulations of not only the ferroelectric instability but also the TiO_6 octahedron rotating instability by the doped carriers are simulated in agreement with experiments, except for the photo-doping effect on the ferroelectric instability in $SrTiO_3$. The modulations of the instabilities were explained by a simple and intuitive mechanism.

They found that the rotation of the TiO_6 octahedron is promoted by doping electrons, while the hole-doping suppresses the rotation. The rotation of the TiO_6 octahedron is induced by the size disagreement between the TiO_2 square and the SrO square. The opposite results of the doping effects between the electron doping and the hole doping is explained by considering the expansion and the shrinking of the radii of the Ti ion and the O ion, and therefore the variation of the ratio of the sizes of the SrO square and the TiO_2 square brought about by them. They pointed out that the modulation of the TiO_6 octahedron rotating instability is, however, too small to be experimentally observed when doped by ≤ 0.001 electrons/10 atoms cell, which is consistent with the previous experiment.

Okuda *et. al.*(2001) [37] investigated transport, thermal, and thermoelectric properties of $Sr_{1-x}La_xTiO_3$ single crystals ($0 \leq x \leq 0.1$). At room temperature Power Factor (PF) (S^2/ρ) 28-38 $\mu W/(K^2 cm)$ were found to be larger that is comparable to that observed in Bi_2Te_3, at relatively high carrier concentrations [(0.2-2) $\dot{x}$ 10^{21} cm^{-3}]. The Seebeck coefficient was well explained by Boltzmann transport model. The unexpectedly large Seebeck coefficients for n > 0.02 per Ti atom ($0.03 * 10^{21}$ cm^{-3}) may be due to the relatively large effective mass, the high (six-fold) degeneracy of the conduction band, and the large scattering parameter (r) in the energy (ε) dependent relaxation time expressed as $\tau = \tau_0 * \varepsilon^{r-1/2}$.

Kong *et. al.*(1999) [38] prepared $La_{0.003}(Sr_xBa_{1-x})_{0.997}$ TiO_3powders by sol-gel process and investigated its electrical properties along with studying the

crystallization by means of XRD and DTA. The results showed that the perovskite phase was formed at 600ºC. Measurement of the lattice parameters for different composition at room temperature showed a decline with x value for $La_{0.003}(Sr_xBa_{1-x})_{0.997}$ TiO_3.The Curie temperatures (T_C) for samples with varying composition and derived from dielectric constant temperature curve decreased with x value. Voltage-current (V-I) property of the samples sintered at 1300ºC was measured. Samples with lowest resistivity tend to show very good nonlinear V-1 property. The conclusion drawn was that Curie temperature for samples decreased with increase in Sr fraction and decreased in Ba composition.

CHAPTER 3

METHODOLOGY

3.1 EXPERIMENTALTECHNIQUES

There has been number of method devised for sample preparation but very limited work has been carried using Sol-Gel method on LSTO. This chapter presents an overview of Sol-Gel method followed by Spark-Plasma Sintering.

3.1.1 Sol-Gel Synthesis Method

The sol-gel firstly developed in the 1960s and expanded to study of perovskite films in the 1980s, the sol-gel field has been expanded to cover almost all wet chemical way to produce thin films and powders over drying and subsequent heat treatment [39]. As the name suggests, there are two different steps during the synthesis.

- The first step is a colloidal suspension of solid particles in the liquid that solution is referred to as the sol. The particles interact with each other in such a way as to generate a polymeric chains which cross-link, creating a three dimensional structure.
- When the structure spreads to the sides of the container and the material becomes rigid enough to resist pouring when inverted, the sol converted into the gel.

If the gel become dry by evaporation, then the effected capillary forces produced and will result in shrinkage, the gel network will breakdown, and a xerogel is formed. If drying is performed under supercritical conditions, the network structure may be retained and a gel with large pores may be formed. This is called an aerogel, and the density will be very low. A record is < 0.005 g/cm^3 [40].

3.1.2 Advantages of Sol-Gel Method

- The sol-gel method prevents the problems with co-precipitation, which may be inhomogeneous, be a gelation reaction.
- Capable for mixing at an atomic level with easy way.
- Formations of small neno-particles, which are easily sinterable.
- Low temperature process (50ºC -600ºC) and easy to maintain.

- One of the greatest important advantages of doped sol-gel materials is their capability for preservation of physical and chemical properties of the doped material.
- Can provide a simple, economic and effective method to produce high quality coatings for thin film.

Sol-gel can be produce high purity products because the organo-metallic precursor of the desired ceramic oxides can be mixed, dissolved in a specified solvent and hydrolyzed into a sol, and subsequently a gel, the composition can be highly controllable [39-40].

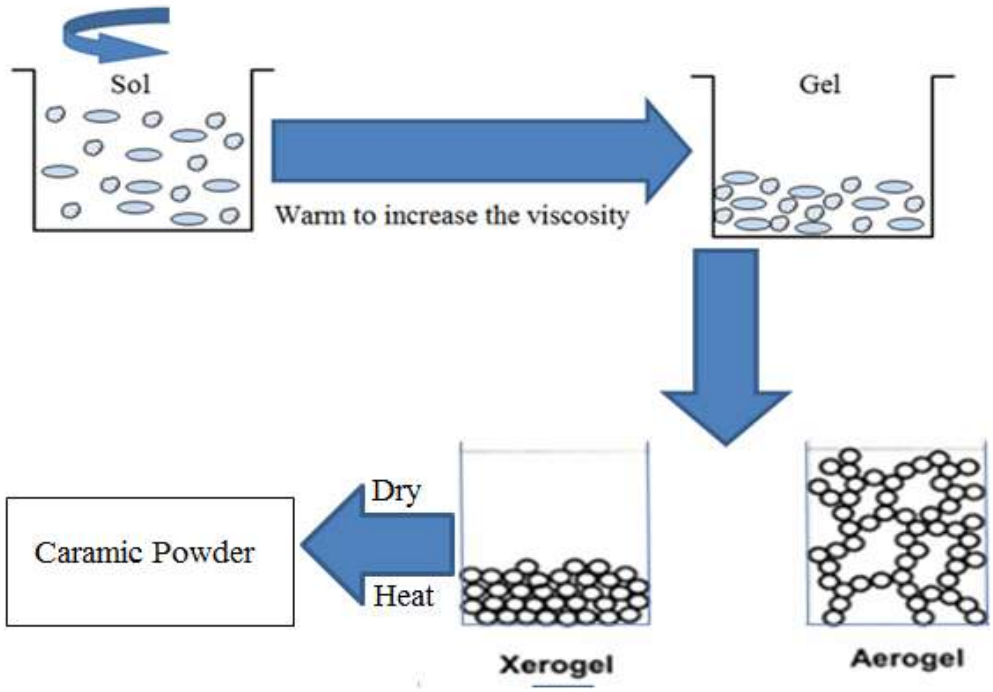

Fig. 3.1 Process diagram of Sol-Gel method.

3.1.3 Synthesis

The sample preparation is the initial step for studies of any solid state compound. There is number of techniques that can be used for synthesis the ceramic compounds, in this research we are going to use sol-gel process. We prepare four sample of $La_xSr_{1-x}TiO_3$ ($La_{0.1}Sr_{0.9}TiO_3$, $La_{0.02}Sr_{0.98}TiO_3$, and $La_{0.04}Sr_{0.96}$ and the last one $La_{0.06}Sr_{0.94}TiO_3$) using sol-gel on the behalf of unique properties of this method, this techniques becomes very popular from recent year because of their low processing temperatures, great chemical homogeneity and the possibility of its controlled particle's size.

La-doped Strontium Titanate prepared from Strontium acetate ($C_4H_6O_7Sr$, Sigma Aldrich) and Lanthanum nitrate hexa-hydrate ($La(NO_3)_3$. $6H_2O$, 99%,Sigma Aldrich) dissolved into acetic acid into two different glass beakers with stirring and heating at 313 to 323 K temperature for 40 min and then mixed them and stirring for 30 min at same temperature. The third solution is Titanium iso-propoxide ($C_{12}H_{28}O_4Ti$, 97%, Sigma Aldrich) dissolved into 2-Methoxyethnol ($C_3H_8O_2$, 99.8%, Sigma Aldrich) heating and stirring in same way and then it dissolved into first solution and stirring for same time and then desire amount of acetyl acetone added to the solution and solution becomes transparent.

Fig. 3.2 Sample synthesis by sol-gel method.

After that solution kept at room temperature for some hours, and then again heating and stirring to make gel and after combustion crush the material to produce the powder form, and the powder placed into furnace for calcinations at 1143 K temperature for few hours.

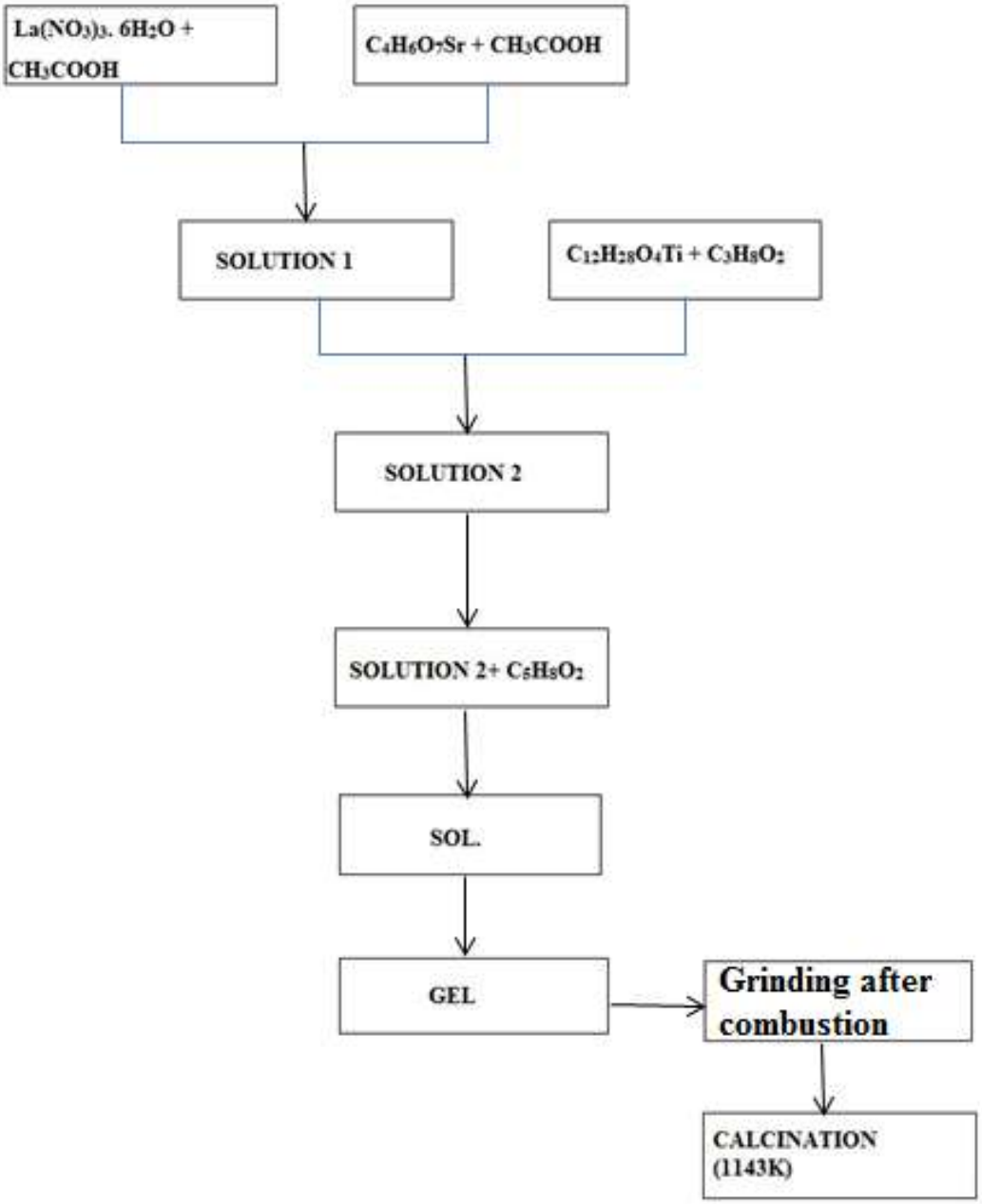

Fig. 3.3 Flow-chart of Sol-Gel Method used for $La_xSr_{1-x}TiO_3$.

3.1.4 Spark Plasma Sintering

Sintering is the process of making pellet for measurement from powder by heating into the furnace below their melting point, in this process bonding takes place by diffusion of atoms. Sintering process can be done by various methods like simple conventional method or by spark plasma sintering (SPS). In this field we are going to use SPS method, the advantages of this method over the conventional method are following:

- SPS method takes few minutes instead of few hours or days as in conventional method for sintering process.
- High heating rate can be attained due to internal heating is 300ºC per min. is very high as comparison of conventional method is maximum 10ºC per min.
- In SPS the nano sized powder sintered without considerable grain growth because of low processing time which is not possible in conventional method therefore by SPS method material can achieved good mechanical properties.

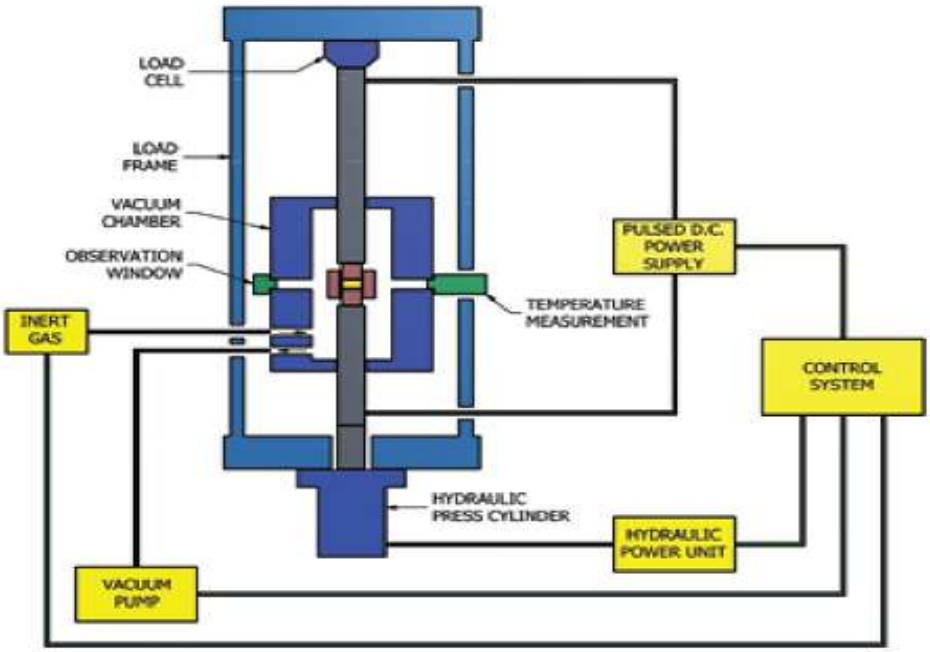

Fig. 3.4 Basic configure of SPS.

In SPS electrical hot press processes use DC or commercial AC power, and main factor that effect the performance of the sintering is joule heat generated by power supply. And because of pressure applied on the sample generate the plastic flow into the material. When the spark discharge at the contact points or in the gap between the powder particles, the high temperature is generated is approximately 10000ºC is responsible of melting and evaporation at surface of particles in SPS sintering [41] is generate neck formation at contact areas or on edge.

3.2 CHARACTERIZATION TECHNIQUES

In order to analyze the samples on nanometer scale one needs to be dependent on highly sophisticated tools like X-Ray Diffraction, Scanning Electron Microscope (SEM), Energy Dispersive X-Ray Spectroscope (EDAX) which can characterize structural, compositional and elemental analysis on a much precise level.

3.2.1 X-Ray Powder Diffraction (XRD)

X-rays were discovered in 1895 by the German physicist Rontgen. Before the discovery of the Bragg's law the X-rays ware applicable for the medical purpose for example inter structure image of bodies, X-rays having very short wave length and form of an electromagnetic radiation with typical energies range of 100 eV -100 keV. The phenomenon of x-rays diffraction by crystal discovered in 1912 which provide a new method to investigation of fine structure of materials. X-Ray diffraction is a versatile and non-destructive investigative method to find out the total information about the molecular bond of crystalline phase and the chemical composition of the material [42]. This is a very effective technique to elaborate and expose the crystal structure of natural and manufactured materials.

Fig. 3.5 X-Ray Diffractometer image.

In this technique the results are compared with the references and standards cards of The International Center for Diffraction (ICDD) and Joint Committee on Powder Diffraction Standards (CPD). These cards contained data from the analyzed materials.

3.2.1.1 Bragg's Law

The X-ray diffraction pattern peaks are indirectly linked to the atomic distances, which are explained in Fig. 3.6 with angle θ signifying the Bragg angle and d referring to the distances between the set of lattice planes:

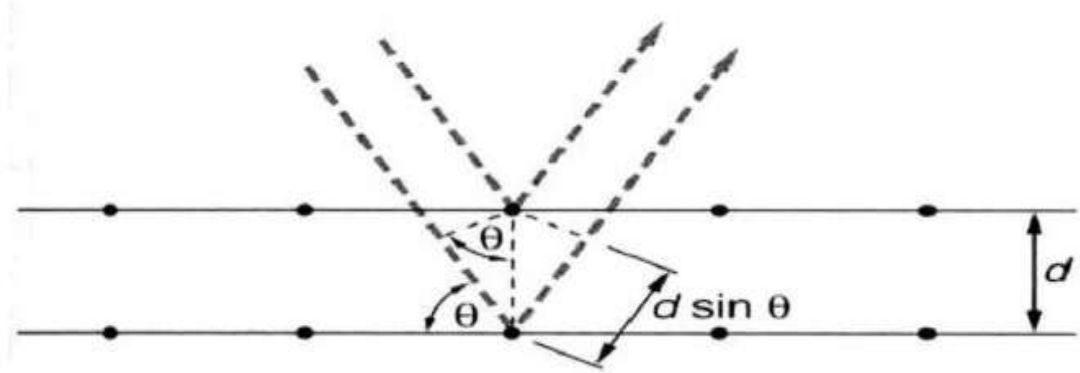

Fig. 3.6 X-rays diffraction from lattice planes.

When two X-rays parallel beams incident on the two atomic layers having interspacing distance d, understandably the one beam travel extra distance 2dsinθ which is equals to the multiplication of the wavelength (λ) and integer (n) for two beam to be faced [43] known as Bragg's law:

$$n\lambda = 2d\sin \times \theta \qquad (3.1)$$

In the Powder X-ray Diffraction (PXRD) pattern the peak positions are correlated to the unit cell parameters and the interatomic layer distance (d), and in the X-ray output the intensities of the peaks are proportional to the square of element's atomic number, a powder form of a sample for the measurement is commonly easy to obtain, which makes PXRD one of the most widely used techniques for characterizing materials. Changes in relative intensity and lattice spacing of diffraction peaks are used to determine the extent of crystallization and changes

in composition or morphology. To calculate average grain size of the sample the Scherrer equation can be used:

$$\tau = \frac{K\lambda}{\beta cos\theta} \tag{3.2}$$

The θ and λ is already defined in Bragg's law and the full width at half of the maximum intensity β in radians is used for a given Bragg's angle to determine average grain size. K (shape factor) supposed to be 0.9 for spherical grains [44]. X-rays diffraction used to determine:

- Crystallite shape from analysis of peak symmetry
- Degree of crystallinity
- Crystallite size from study of peak broadening
- Crystal structure and crystalline phase

3.2.2 Scanning Electron Microscopy (SEM)

The SEM is one of the most versatile instruments available for the examination and analysis of the microstructural characteristics of solid objects. The scanning electron microscope capable to very low magnification (about 10X) to 50000X and resolution about 10mm (100 Å). So because of its high morphological properties we can use it to count particle range 1mm to 0.1µm.Scanning Electron microscope has depth of field 300 times more than optical microscope. The output image is generated by the secondary electrons when narrow electrons beam with high intensity strike on the sample surface. Scanning Electron microscope has depth of field 300 times more than optical microscope. The output image is generated by the secondary electrons when narrow electrons beam with high intensity strike on the sample surface. The image contrast depends upon the topography of the sample so the prepared powders must not embedded in film but dispersed on smooth substrate [45].

For scanning electron microscopy JEOL JSM-6510LVSEM with a high resolution of 3.0 nm at 30 kV was used, the JEOL JSM-6510LV SEM image is shown in Fig. 4.3.The STO is a non-conducting ceramic material, so it is necessary to use coating on the surface of the material to make it conducting.

Fig. 3.7 Scanning Electron Microscopy

The STO material was coated with the gold plating with JEOL JFC auto fine coater. EDS (Electron Dispersive Spectroscopy) is an investigative technique used for the chemical characterization or elemental analysis of a sample. It relies on the examination of an interaction of X-ray excitation and a sample surface.

CHAPTER 4

RESULT AND DISCUSSIONS

This chapter deals with the results obtained from different experiments performed. The route followed for synthesis of ceramic using novice sol gel method has been discussed in details followed by its characterization. The micrographs and diffraction curves obtained from SEM analysis and XRD analysis respectively have been thoroughly analyzed to draw some solid conclusion. The EDS analysis was carried out for chemical characterization and elemental analysis of the ceramic under investigation.

4.1 XRD ANALYSIS

Fig. 4.1 shows the XRD diffractogram of $La_xSr_{(1-x)}TiO3$ (x = 0.10, 0.02, 0.04, 0.06). It was observed that the crystalline size area declined with addition of lanthanum with $La_{0.02}$ Sr $_{0.98}$ TiO_3 showing the larger crystalline size and $La_{0.10}Sr_{0.9}TiO_3$ shows the smallest crystalline size among all the samples. The exact value of crystalline size for every sample with varying Lanthanum doping (i.e. x value) has been tabulated in Table 4.1.

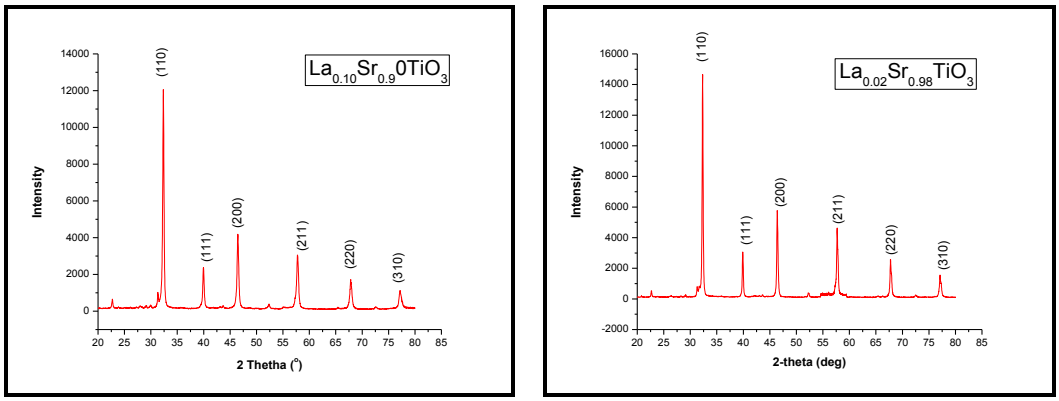

(a) (b)

Fig 4.1 XRD Diffrectogram (a) $La_{0.1}Sr_{0.90}TiO_3$ (b) $La_{0.02}Sr_{0.98}TiO_3$

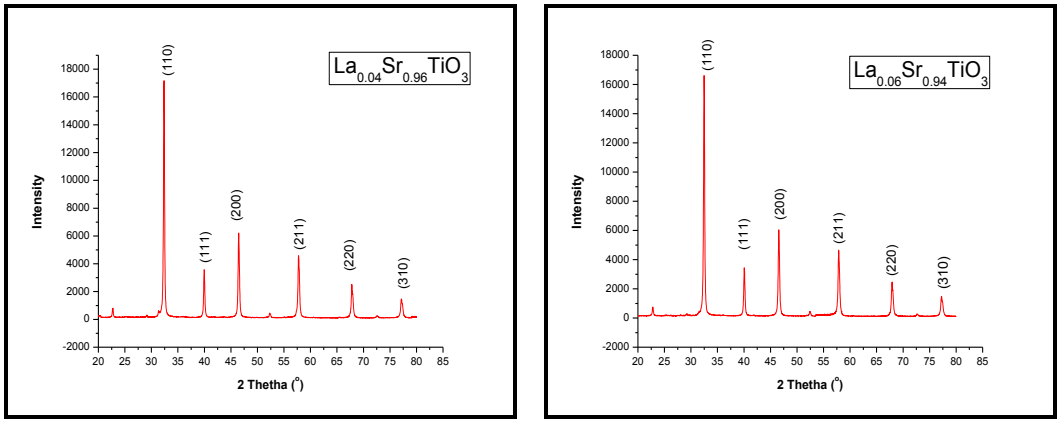

(c) (d)

Fig. 4.1 XRD Diffrectogram for (c) $La_{0.04}Sr_{0.96}TiO_3$ (d) $La_{0.06}Sr_{0.98}TiO_3$

From the XRD analysis we found that the crystalline size is decreases with respect to increasing the doping composition as shown in Table 4.1, the crystalline size is decreased from 40.3 (at x = 0.02) to 35.8 (at x = 0.1) in $La_xSr_{(1-x)}TiO_3$. On the other hand the lattice parameter is also shows the same pattern. For composition $La_{0.02}$ Sr $_{0.98}$ TiO_3 the lattice parameter is 3.9118 and it is decreasing with respect to the increasing lanthanum doping as in $La_{0.10}Sr_{0.9}TiO_3$ is 3.9093.

Table 4.1 Variation of crystalline size and lattice parameter with composition

Composition	Crystalline Size (nm)	Lattice Parameters (Å)
$La_{0.02}Sr_{0.98}TiO_3$	40.3	3.9118
$La_{0.04}$ Sr $_{0.96}$ TiO_3	39.0	3.9073
$La_{0.06}$ Sr $_{0.94}$ TiO_3	37.8	3.8996
$La_{0.10}$ Sr $_{0.9}$ TiO_3	35.8	3.9093

The major peaks for all LSTO samples are indexed and lattice parameters are same a = b = c shows cubic structure format at all composition of La doping. The XRD pattern shows that the sample contained very minor impurity peaks and match with JCPDS card number 00-035-0795. The pattern in the Fig. 4.1 shows the clear single cubic phase without any secondary phase.

4.2 SEM ANALYSIS

The SEM micrograph for powder form of lanthanum doped Strontium titanate is shown in Fig 4.2. In the all micrograph the particle size is distributed in random size, the average particle size calculated for sample 2.1 µm for sample $La_{0.1}Sr_{0.90}TiO_3$ shown in Fig. 4.2 (a), the average particle measured for sample $La_{0.02}Sr_{0.98}TiO_3$ is 1.2 µm shown in Fig. 4.2 (b) and calculated particle size for $La_{0.04}Sr_{0.96}TiO_3$ and $La_{0.06}Sr_{0.94}TiO_3$ are 1.3 µm and 2.8 µm (Fig. 4.2 (c) and (d)).

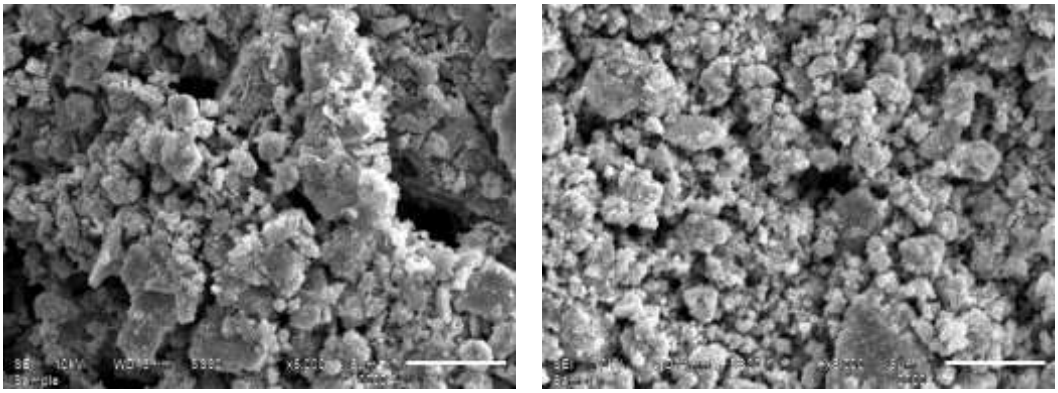

(a) (b)

Fig. 4.2 SEM Micrograph image (a) $La_{0.1}Sr_{0.90}TiO_3$, (b) $La_{0.02}Sr_{0.98}TiO_3$

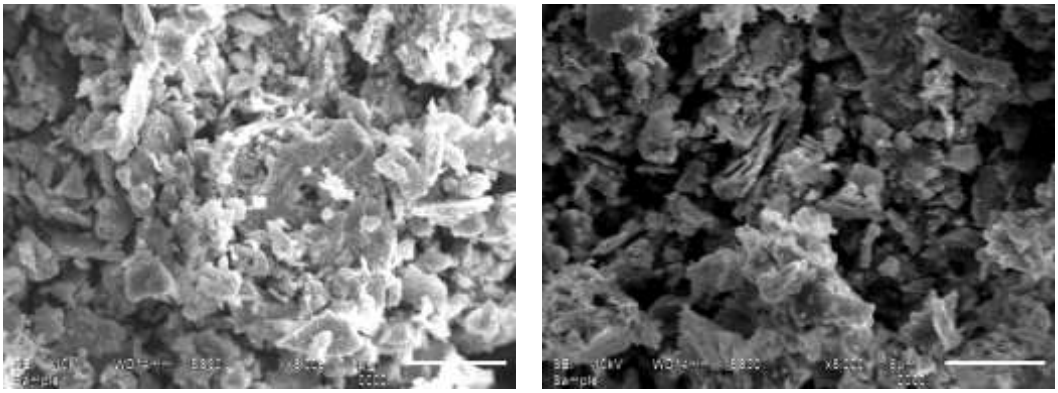

(c) (d)

Fig. 4.2 SEM Micrograph image (c) $La_{0.04}Sr_{0.96}TiO_3$ and (d) $La_{0.06}Sr_{0.94}TiO_3$

On comparing the micrograph of sample sintered at different temperature that can see in Fig. 4.3 and 4.4. The pellet which was sintered at temperature 1200^{o}C

showing fine grain growth, have less porosity and good compactness as compared to the pellet sintered at 1000^{o}C.

The grain size is approximately 1.2 µm for the pellet sintered at 1200^{o}C has been found and on the other hand the grain size 0.5 µm can be observed for the pellet sintered at 1000^{o}C.

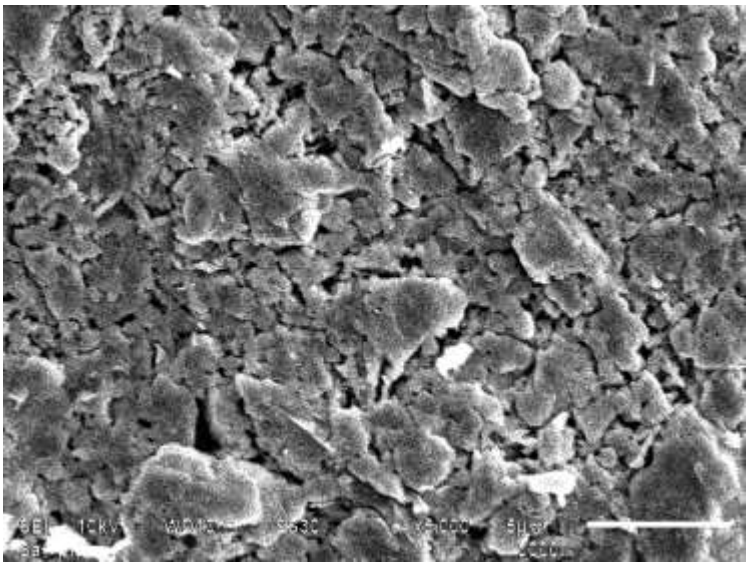

Fig. 4.3 Micrograph of $La_{0.06}Sr_{0.94}TiO_3$ with spark plasma sintering at 1200 ^{o}C

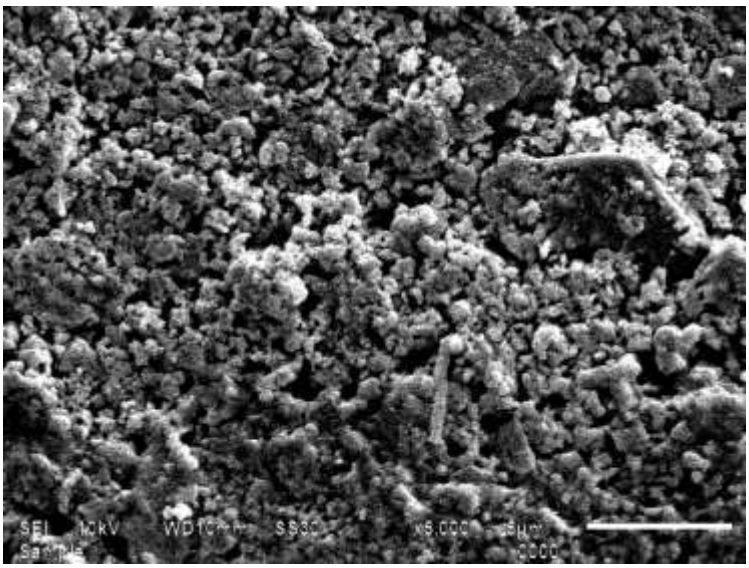

Fig. 4.4 Micrograph of $La_{0.02}Sr_{0.98}TiO_3$ with Spark Plasma Sintering at 1000^{o}C

The surface morphology of the pellet sintered at higher temperature is more ordered and porosity is less.

Due to better surface morphology the pellet sintered at higher temperature may have better mechanical behavior. This is one of the better criteria for applying the material to thermoelectric devices.

4.3 EDS Analysis

The EDS analysis was carried out in order to determine the elements present in samples being fabricated in present study. Fig. 4.5 (a), 4.5 (b), 4.5 (c), 4.5 (d) shows EDS spectrum of $La_xSr_{(1-x)}TiO_3$, $La_{0.02}Sr_{0.98}TiO_3$, $La_{0.04}Sr_{0.96}TiO_3$, $La_{0.06}Sr_{0.94}TiO_3$ respectively.

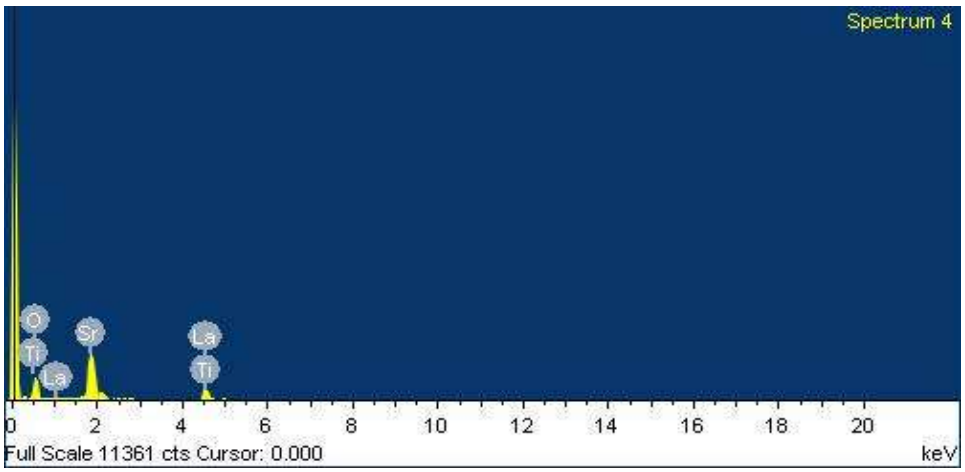

Fig. 4.5 (a) EDS Spectrum of $La_{0.1}Sr_{0.9}TiO_3$

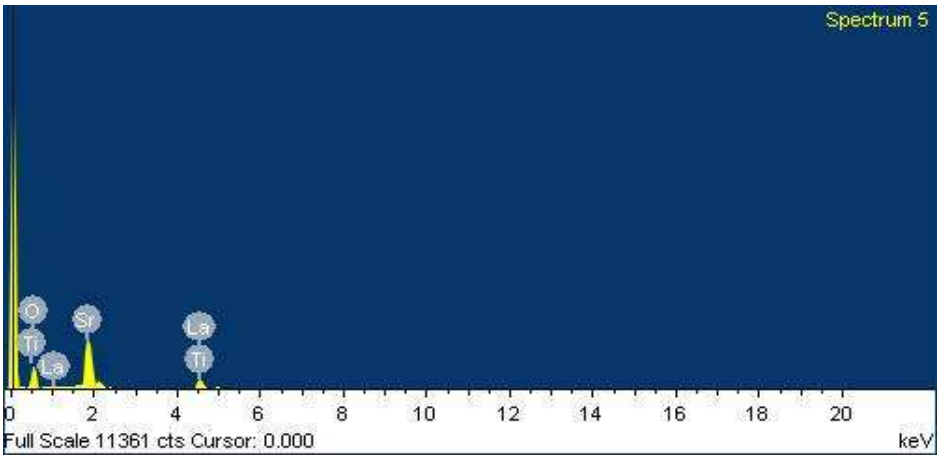

Fig. 4.5 (b) EDS Spectrum of $La_{0.02}Sr_{0.98}TiO_3$

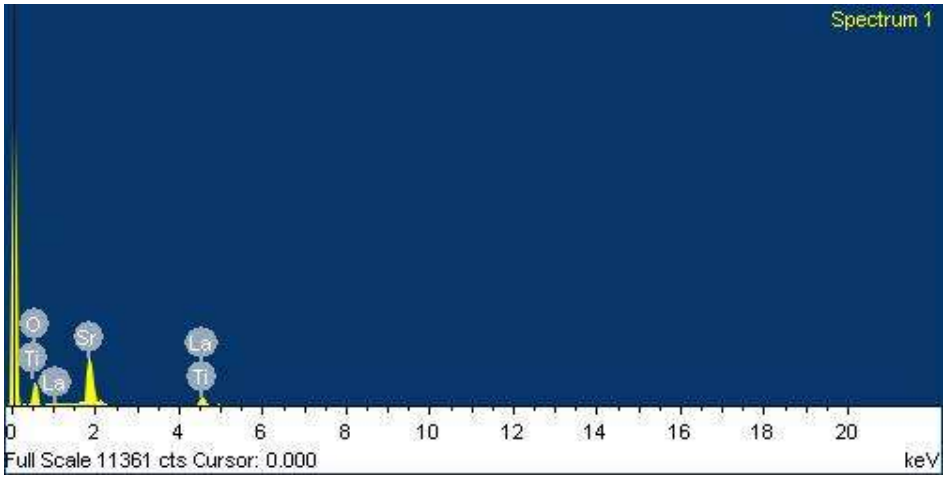

Fig. 4.5 (c) EDS Spectrum of $La_{0.04}Sr_{0.96}TiO_3$

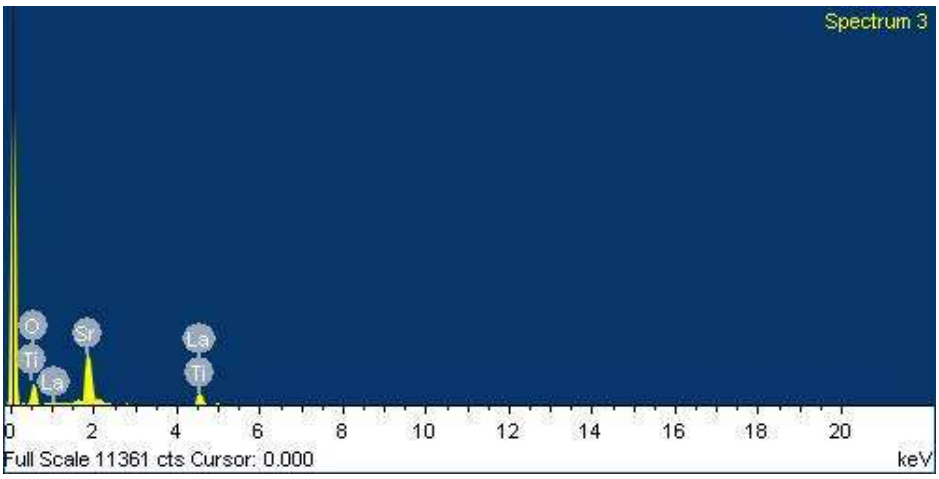

Fig. 4.5 (d) EDS Spectrum of $La_{0.06}Sr_{0.94}TiO_3$

The molecular ratio of (La + Sr)/Ti have been found to be approximately equal to 1 for all samples (Table 4.2). Though it is clearly equal to 1, but the EDS have confined the stoichiometric ratio and the present of all the involved element is found in the system.

Table 4.2 Stoichiometric composition with varying composition

Composition	Ratio of (La + Sr)/ Ti
$La_{0.10}$ Sr $_{0.9}$ TiO_3	**1.126**
$La_{0.06}$ Sr $_{0.94}$ TiO_3	**1.052**
$La_{0.04}$ Sr $_{0.96}$ TiO_3	**0.983**
$La_{0.02}$ Sr $_{0.98}$ TiO_3	**0.969**

CHAPTER 5

CONCLUSIONS

5.1 CONCLUSION

i. The samples of LSTO ($La_xSr_{(1-x)}TiO_3$) with different varying composition ($La_{0.1}Sr_{0.9}TiO_3$, $La_{0.02}Sr_{0.98}TiO_3$, $La_{0.04}Sr_{0.96}TiO_3$ and $La_{0.06}Sr_{0.94}TiO_3$) has been Synthesized successfully by Sol Gel route.

ii. From the XRD analysis confirmed that all samples has single phase cubic structure for all value of x (0.1, 0.02, 0.04, 0.06) and lattice parameter for these values of x is found 3.9093Å, 3.9118 Å, 3.9073 Å and 3.8996 Å. And crystalline size 35.8 nm, 40.3nm, 39.0 nm and 37.8 for $La_xSr_{1-x}Ti_{O3}$.

iii. According to SEM morphological structure with average grain size of the particles around 1μm and pellets prepared by Spark Plasma Sintering shows that with sintering 1200^oC have less porosity and good compactness as compared to sintered at 1000^oC, therefore only high temperature sintering is required for further LSTO application purpose.

iv. EDS have confined the stoichiometric ratio and the present of all the involved element is found in the system.

5.2 FUTURE SCOPE

- Although it is one of the good material for thermal electric devices, but high temperature sintering is required for that application. So its thermoelectric behavior (seeback coefficient (S), figure of merit (ZT), power factor (PF), electrical conductivity (σ), thermal conductivity (k), carrier concentration) should be studied after performing high temperature sintering.
- These materials are also good solid state electrolyte. Hence they can be applied for the devices based on ion transfer to such as gas sensor, SOFC and batteries *etc.*
- The dielectric and optical property of LSTO could be useful for modern electronics applications and hence a deep investigation in this direction is required.

REFERENCES

[1] V. S. Arunachalam and E. L. Fleischer, MRS Bull **33**, 264 (2008).

[2] R. H. Mitchell and T. Bay, Almaz Press Inc., **7**, 96 (2002).

[3] P. M. Woodward, Acta Crystallogr., B **53**, 32 (1997).

[4] L. Cai, A. L. Arias and J. C. Nino, J. Mater. Chem., **21**, 3611(2011).

[5] K. Koumoto, Y. Wang, R. Zhang, A. Kosuga, and R. Funahashi., Annu. Rev. Mater. Res., **40**, 365 (2010).

[6] T. Fang, Phys. Rev. B, **25**, 627 (1982).

[7] Z. Yuand C. Ang, Appl. Phys. Lett., **80**, 643 (2002).

[8] H. Suzuki, J. Phys. Soc. Jpn., **65**, 1529(1996).

[9] R.D. Leapman, L.A. Grunes and P.L. Fejes, Phys. Rev., B **26**, 614 (1982).

[10] K. Uchida, S. Tsuneyuki, and T. Schimizu, Phys. Rev., B **68**, 174107 (2003).

[11] F. A. Cotton, John Wiley & Sons, New York **3**, (1990).

[12] K.W. Blazey, Phys. Rev. Lett., **27**, 146 (1971).

[13] E. Scheneider, P. J. Cressman and R. L. Holman, J. Appl. Phys., **53**, 4054 (1982).

[14] R. D. Shannon, Acta Crystallogr., A **32**, 751 (1976).

[15] N. H. Chan, R. K. Sharma, and D. M. Smyth, J. Electrochem. Soc., **128**, 1762 (1981).

[16] R. M. Ormerod, Chem. Soc. Rev., **32**, 17 (2003).

[17] J. W. Fergus, Sens. Actuators, B-Chem., **123**, 1169 (2007).

[18] W. J. Dawson, Am. Ceram. Soc. Bull., **67**, 1673 (1988)

[19] R. Roy, J. Solid State Chem. **111**, 11 (1994).

[20] K. M. Doxsee, Chem. Mater. **10**, 2610 (1998).

[21] S.L. Swartz,S. D. Ramamurthi, J. R. Busch and V. E. Wood, MRS Proc., **243**, 530 (1991)

[22] F. Bezzi, A. L. Costa, D. Piazza, A. Ruffini, S. Albonetti and C. Galassi, J. Euro. Ceram. Soc., **25**, 3323(2005).

[23] J.V. Biggers, S. Venkataramani, Mater. Res. Bull. **13**, 717 (1978)

[24] W. L. Suchanek and R. E. Riman, Adv. Sci. Tech. **45**, 184 (2006).

[25] J. Liu, C.L. Wang, H. Peng, W. B. Su, H.C. Wang, J. C. Li, J. L. Zhang, and L. M. Mei, J. Electron. Mater., **41**, 373 (2012).

[26] R. Sun, D. Li, L. Li, J. Zhang, Q. Wang, X. Qin, Proc. Eng., **27**, 103 (2012).

[27] H.C. Wang, C. L. Wang, W. B. Su, J. Liu, Y. Sun, H. Peng, and L. M. Mei, J. Am. Ceram. Soc., **94**, 838 (2011).

[28] X. Wang, X. Lu, Y. Weng, W. Cai, X. Wu, Y. Liu, F. Huang, J. Zhu, Solid State Commus., **150**, 267 (2010).

[29] N. Okinaka, L. Zhang and T. Akiyama, ISIJ Int., **50**, 1300-1304 (2010).

[30] A. Kikuchi, L. Zhang, N. Okinaka, T. Tosho and T. Akiyama., Mater. Trans., **51**, 1919 (2010).

[31] A. Kinaci, C. Sevik and T. Çagın, Phys. Rev. B **82**, 155114 (2010).
[32] A. Kikuchi, L. Zhang, N. Okinaka, T. Tosho, and T. Akiyama, Mater. Trans., **50,** 2675 (2009).
[33] J. Liu, C. L. Wang, W. B. Su, H. C. Wang, P. Zheng, Appl. Phy. Lett. **95**, 162110 (2009)
[34] Y.F. Yamada, A. Ohtomo and M. Kawasaki, Appl. Surf. Sci. **254**, 768 (2007).
[35] F. Voigts, T. Damjanovic, G. Borchardt, C. Argirusis, and W. M. Friedrichs, J. Nanomater., **54**, 1 (2006).
[36] S. Ohta, T. Nomura, H. Ohta, K. Koumoto, J. Appl. Phys., **97**, 034106 (2005).
[37] T. Okuda, K. Nakanishi, S. Miyasaka and Y. Tokura, Phys. rev. B **68**, 113104 (1999).
[38] L. Kong, X. Yao and L. Zhang, Ferroelectr., **234**, 211 (1999).
[39] J. Livage, M. Henry and C. Sanchez, Progress in Solid State Chem., **18**, 259 (1988).
[40] J. L. Gourav, I. K. Jung, H. H. Park, E. S. Kang, D. Y. Nadaargy, J. Nanomater., **2010**, 1 (2010).
[41] C. H. Hsueh and P. Miranda, J. Mater. Res. **18**, 5 (2003).
[42] M.Tokita, J. Kana. Sci., **108**, 1 (1999).
[43] W. L. Bragg, Proc. Camb. Philos. Soc., **17**, 43 (1913).
[44] L. E. Smart and E. A. Moore, CRC Press, **3**, 332(2005).
[45] K.C.A. Smit, J. Appl. Phys., **6**, 399 (1955).

CURRICULAM VITAE

DHARAM PAL Mobile: +91-9815934602

M Tech. THAPAR UNIVERSITY Email – dh_dehal@ymail.com

A Mechanical Engineer trained in Quality Assurance AND Designing with experience of a 1YR.

- Proficient in Quality Assurance, Designing
- Skilled in using Quality Tools like MSA (Measuring System Analysis), 5S, KAIZEN, Control Charts, Check Sheets
- Skilled in Process Capability.
- Proficient in CAD2007 CATIA V5R19 and First Piece Approval and In-process Inspection.
- Skilled in Product Development process including finalizing CONTROL PLANS, PPAP.

Professional Experience

Work with **ARVIND TALWAR MACHINE TOOLS PVT. LTD.,** UNA, H.P since July, 2010 to July, 2011.

Technical skills

- Engineering Concepts : Design and Quality Engineer
- Software Skills : CMM using MiCAT Geopak, AutoCad 2007,CATIA V5R19
- Operating System : Windows98/2000/XP7
- Product Development : Control Plans, PPAP (Part Process Approval Plan).

Educational Details

COURSE	YEAR OF PASSING	SUBJECT/ SPECIALIZATION	INSTITUTION	BOARD/ UNIVERSITY
Masters	2011-2013	Metallurgical Engg.	*7.2/10(till 3rd sem)*	Thapar University
Graduation	2006-2010	Mechanical Engg.	*60.1%*	Punjab Technical University

Project Experience

Projects (Arvind Group)

Project # 1:

- **Project Title – Designing and manufacturing of jigs and fixtures**

Project Details–development of 39 components for ashok leyland required designing and manufacturing of jigs and fixtures for various jobs according to requirement of various components and processes jigs and fixtures have been designed and manufactured.

Responsible for –

- Planning jigs and fixtures requirement for various components.
- Drafting 2D drawing for jigs and fixtures
- Supervising the fabrication of jigs and fixture according to the drawings

Training Details

Name of Institution	Course	Year.
SHAHEED BHAGAT SINGH COLLEGE OF ENGG. & TECHNOLOGY, Ferozepur- Punjab	4 Weeks WORKSHOP TRAINING	2007
NATIONAL FERTILIZERS LTD., NayaNangal, Distt. Ropar, Punjab-140126	6 Weeks INDUCTION TRAINING (Maintenance Deptt. , Mechanical Workshop)	2008
International car and motors ltd.(sonalika) ambdisttuna hp	6 Months INDUSTRIAL TRAINING	2009

Extra Curricular Activities

1. Served as Joint Secretary, Public Relation Officer & General Secretary for "Society for Extra Curricular Activities" (SECA) in the college.
2. Worked as Senior Executive in "Society for Mechanical Engineers" (SFME).
3. Captain of college kabaddi team.

Personal Profile

Address for communication : VPO Dehlan Distt. & Teh una (HP)

Date of birth : 20th sep. 1987
Mobile : +91-9815934602